

Enhancing Language Models for Robust Greenwashing Detection

Neil Heinrich Braun¹, Keane Ong^{1,2}, Rui Mao³, Erik Cambria³, Gianmarco Mengaldo¹

¹National University of Singapore, ²Massachusetts Institute of Technology, ³Nanyang Technological University

Abstract

Sustainability reports are critical for ESG assessment, yet greenwashing and vague claims often undermine their reliability. Existing NLP models lack robustness to these practices, typically relying on surface-level patterns that generalize poorly. We propose a parameter-efficient framework that structures LLM latent spaces by combining contrastive learning with an ordinal ranking objective to capture graded distinctions between concrete actions and ambiguous claims. Our approach incorporates gated feature modulation to filter disclosure noise and utilizes MetaGradNorm to stabilize multi-objective optimization. Experiments in cross-category settings demonstrate superior robustness over standard baselines while revealing a trade-off between representational rigidity and generalization.¹

1 Introduction

Sustainability reports are key to evaluating corporate ESG performance, but their credibility is increasingly undermined by greenwashing, where vague or inflated claims blur the line between real action and rhetoric (Pimonenko et al., 2020). Although NLP systems are widely used to analyze these disclosures, they remain vulnerable to strategically crafted language (Ong et al., 2025b). Current models often over-rely on surface-level lexical and stylistic patterns, leading to strong in-distribution performance but poor generalization to unseen categories or shifted formulations. Crucially, increasing model capacity does not consistently improve robustness in this setting. This limitation is particularly problematic for ESG analysis, as companies can strategically alter their reporting focus or linguistic framing without changing underlying sustainability practices, requiring models

that can look beyond surface-level cues to identify substantive actions (Stammbach et al., 2023).

A key source of model fragility is that ESG analysis is typically framed as a flat prediction problem, optimizing a single objective without imposing structure on the latent representation space (Ong et al., 2025b). Consequently, critical distinctions such as degrees of actionability, commitment, or evidential grounding are not explicitly encoded. Since greenwashing emerges from nuanced combinations of intent and substantiation rather than isolated cues, we hypothesize that robustness can be improved by explicitly structuring latent representations during fine-tuning (Stoehr et al., 2023). By explicitly encoding ordinal relationships between concrete actions and ambiguous claims, models may better capture underlying intent. Yet, enforcing such structure introduces a trade-off where rigid constraints potentially limit generalization to unseen cases.

We propose a parameter-efficient framework that applies structured representation learning directly to low-rank adapters (LoRA). Our approach integrates a contrastive objective to cluster semantically related claims with an ordinal ranking loss to enforce graded distinctions of actionability. A gated feature modulation mechanism further mitigates noise by dynamically emphasizing task-relevant dimensions. To stabilize the resulting multi-loss optimization, we introduce MetaGradNorm, which automatically balances competing gradients and loss contributions to ensure robust convergence without manual tuning (Chen et al., 2018).

We evaluate our framework on the A3CG dataset (Ong et al., 2025b) using a cross-category generalization setting across several open-source LLMs: T5 (Raffel et al., 2020), LLaMA-3-8B (Llama Team, AI @ Meta, 2024), Mistral-7B (Jiang et al., 2023), Gemma-7B (Gemma Team et al., 2024), DeepSeek-V3-7B (DeepSeek-AI et al.,

¹Code will be released upon review.

2024a), and Qwen2.5-7B (Qwen et al., 2024). Our key findings include: (1) While T5 achieves the strongest overall performance, our framework consistently improves robustness across all other LLMs. (2) For these medium-scale models, structured fine-tuning yields higher robustness than 70B-parameter variants and proprietary systems, suggesting that representation structure is more critical than model scale. (3) Despite these gains, simple LoRA remains a highly competitive and consistent baseline across settings. (4) Finally, we discuss remaining limitations and outline future research strategies.

Our main contributions are as follows: (1) A structured PEFT framework that integrates contrastive and ordinal representation learning directly into low-rank adapters for robust ESG claim analysis. (2) A gated feature modulation mechanism to filter noise and strategic language in sustainability disclosures by dynamically emphasizing task-relevant dimensions. (3) MetaGradNorm, an optimization strategy that adaptively balances competing objectives to stabilize multi-loss training in structured representation settings. (4) A comprehensive empirical evaluation of robustness and generalization trade-offs across multiple LLMs and ESG categories, identifying key scaling and structural limitations.

2 Related Work

NLP for ESG Analysis and Greenwashing While NLP has been extensively applied to ESG disclosure analysis for tasks such as sustainability topic extraction (Ong et al., 2025c) and structured information extraction (Song et al., 2018; Bronzini et al., 2024), the strategic ambiguity inherent in greenwashing remains a fundamental challenge (Ong et al., 2025a). Recent shifts toward the Aspect–Action Modeling and Cross-Category Generalization (A3CG) framework address this by linking ESG aspects to specific corporate actions categorized along an ordinal continuum of commitment - ranging from indeterminate to implemented (Ong et al., 2025b). Despite the rise of Large Language Models (LLMs) in this domain, scaling alone has proven insufficient for fine-grained sustainability analysis; proprietary models often struggle with the cross-category generalization and linguistic sensitivity required to distinguish rhetorical patterns from credible actions (Ong et al., 2025b; Bronzini et al., 2024).

Parameter-Efficient Fine-Tuning for LLMs. While methods like LoRA (Hu et al., 2022) reduce computational costs by adapting models via low-rank matrices (Han et al., 2024; Lialin et al., 2023), they typically rely on standard supervised objectives that do not explicitly structure the representation space. Consequently, these techniques often struggle with robustness and generalization in complex tasks due to a lack of mechanisms for encoding task-aligned constraints during adaptation.

Contrastive Learning for NLP Representation Learning Contrastive learning enhances representation quality by clustering semantically similar instances while separating dissimilar ones, improving robustness in sentence and aspect-based tasks (Wang and Isola, 2020; Gao et al., 2021). However, its effectiveness depends heavily on hyperparameter tuning (e.g., margin, temperature). Furthermore, rigid contrastive constraints can hinder generalization if the training data’s semantic structure fails to align with unseen distributions (Huang et al., 2023).

Ordinal and Structured Objectives in NLP Beyond contrastive learning, ordinal regression and ranking-based losses capture graded relationships - such as sentiment intensity or stance - that discrete labels miss (Stoehr et al., 2023; He et al., 2016). While these objectives improve interpretability and alignment by encoding relative distinctions, integrating them into multi-objective pipelines is difficult. Furthermore, enforcing such structures can introduce rigidity, potentially limiting performance on ambiguous or unseen cases (Baly et al., 2019).

Gating Mechanisms for Feature Modulation Gating mechanisms dynamically modulate information flow by selectively emphasizing task-relevant features, which improves robustness in NLP tasks with noisy or heterogeneous inputs — such as aspect-based sentiment analysis and domain adaptation (Xue and Li, 2018; Veyseh et al., 2020). In ESG analysis, where boilerplate obscures signals, feature-level gating offers a principled way to attenuate irrelevant dimensions while amplifying representations of meaningful sustainability actions. (Quan et al., 2024).

Multi-Objective Optimization and Loss Balancing Multi-objective training often suffers from competing gradients and imbalanced dynamics,

where fixed weighting schemes allow a single objective to dominate or destabilize training (Chen et al., 2018; Yu et al., 2020). To mitigate this, adaptive methods like GradNorm dynamically adjust weights based on gradient magnitudes, while meta-learning extensions further stabilize learning (Mao et al., 2022). These strategies are essential in frameworks combining supervised, contrastive, and structured objectives to ensure balanced convergence across different loss scales.

3 Methodology

3.1 Task Definition and Problem Setup

We study ESG claim analysis under an aspect–action formulation, where each claim is represented as a tuple pairing a sustainability aspect with an associated action description. The action component captures how the aspect is operationalized, from abstract commitments to concrete, verifiable actions. Following prior work on aspect–action modeling (Ong et al., 2025b), actions are organized along an ordinal continuum of increasing actionability. Each claim is assigned an ordinal label $y \in \{indeterminate, planning, implemented\}$, reflecting progressively stronger evidential grounding. The objective is to learn representations that preserve these ordinal relationships while generalizing across unseen ESG categories.

3.2 Embedding Extraction and Similarity Functions

Let f_θ denote a pretrained language model with parameters θ . Given an input claim x , we extract a latent embedding $x \in \mathbb{R}^d$, which is L2-normalized as:

$$\hat{x} = \frac{x}{\|x\|_2}. \quad (1)$$

We define cosine similarity and distance as:

$$\text{sim}(u, v) = \hat{u}^\top \hat{v}, \quad \hat{d}(u, v) = 1 - \text{sim}(u, v), \quad (2)$$

which are used consistently across all objectives.

3.3 Parameter-Efficient Adaptation with LoRA

We employ Low-Rank Adaptation (LoRA) (Hu et al., 2022) and use the same LoRA adapters across both structured representation learning and subsequent PEFT fine-tuning, ensuring continuity of the learned latent space. Adapters are injected into the attention projections and the feed-forward projections.

3.4 Contrastive Representation Learning

To structure the latent space, we employ supervised contrastive learning (Khosla et al., 2020). For each anchor embedding a , we consider a set of positive samples $\{p_k\}_{k=1}^K$ and negative samples $\{n_m\}_{m=1}^M$. Using cosine similarity $\text{sim}(\cdot, \cdot)$ and temperature $\tau > 0$, we define the multi-positive contrastive loss as:

$$\mathcal{L}_{\text{ctr}}^{(i)} = -\log \frac{\sum_{k=1}^K \exp(\text{sim}(a, p_k)/\tau)}{\sum_{k=1}^K \exp(\text{sim}(a, p_k)/\tau) + \sum_{m=1}^M \exp(\text{sim}(a, n_m)/\tau)} \quad (3)$$

This objective encourages semantically related claims to cluster in the latent space while separating unrelated ones.

3.5 Ordinal Ranking Objective

While contrastive learning enforces similarity structure, it does not explicitly encode ordinal relationships between action levels. To address this limitation, we introduce an ordinal ranking objective aligned with the actionability continuum in A3CG (Stoehr et al., 2023).

For each anchor, we define an ordinal mean-margin loss with a constant margin $m_0 > 0$:

$$\mathcal{L}_{\text{ord}}^{(i)} = \max \left(0, \frac{1}{K} \sum_{k=1}^K \hat{d}(a, p_k) - \frac{1}{M} \sum_{m=1}^M \hat{d}(a, n_m) + m_0 \right) \quad (4)$$

This loss enforces that higher-actionability claims remain closer to the anchor than lower-actionability ones by a fixed margin, aligning representation geometry with the ordinal action scale.

3.6 Per-Sample Gating Mechanism

To balance contrastive and ordinal objectives at the sample level, we introduce a gating mechanism with temperature parameters $T_{\text{ctr}}, T_{\text{ord}} > 0$. For each sample i , we compute:

$$s_{\text{ctr}}^{(i)} = \frac{\mathcal{L}_{\text{ctr}}^{(i)}}{T_{\text{ctr}}} - \frac{\mathcal{L}_{\text{ord}}^{(i)}}{T_{\text{ord}}}, \quad s_{\text{ord}}^{(i)} = \frac{\mathcal{L}_{\text{ord}}^{(i)}}{T_{\text{ord}}} - \frac{\mathcal{L}_{\text{ctr}}^{(i)}}{T_{\text{ctr}}}. \quad (5)$$

Normalized gating weights are obtained via:

$$(w_{\text{ctr}}^{(i)}, w_{\text{ord}}^{(i)}) = \text{softmax}(s_{\text{ctr}}^{(i)}, s_{\text{ord}}^{(i)}), \quad w_{\text{ctr}}^{(i)} + w_{\text{ord}}^{(i)} = 1. \quad (6)$$

3.7 Multi-Objective Learning and Loss Balancing

The batch-level objective is defined as:

$$\mathcal{L}(\theta; \alpha) = \frac{1}{B} \sum_{i=1}^B \left[\lambda_{\text{base}} w_{\text{ctr}}^{(i)} \mathcal{L}_{\text{ctr}}^{(i)} + \lambda_{\text{ord}} w_{\text{ord}}^{(i)} \mathcal{L}_{\text{ord}}^{(i)} \right] \quad (7)$$

where $\alpha = \{\lambda_{\text{base}}, \lambda_{\text{ord}}, T_{\text{ctr}}, T_{\text{ord}}\}$ are meta-parameters.

3.8 MetaGradNorm for Loss Balancing

To stabilize multi-objective training, we adopt a MetaGradNorm strategy derived from GradNorm (Chen et al., 2018). Gradient norms are computed as:

$$\begin{aligned} G_{\text{ctr}} &= \left\| \nabla_{\theta} \left(\frac{1}{B} \sum_i \lambda_{\text{base}} w_{\text{ctr}}^{(i)} \mathcal{L}_{\text{ctr}}^{(i)} \right) \right\|_2, \\ G_{\text{ord}} &= \left\| \nabla_{\theta} \left(\frac{1}{B} \sum_i \lambda_{\text{ord}} w_{\text{ord}}^{(i)} \mathcal{L}_{\text{ord}}^{(i)} \right) \right\|_2. \end{aligned} \quad (8)$$

Normalized losses define difficulty ratios:

$$\tilde{L}_k(t) = \frac{L_k(t)}{L_k(0) + \varepsilon}, \quad r_k(t) = \left(\frac{\tilde{L}_k(t)}{\frac{1}{2} \sum_j \tilde{L}_j(t)} \right)^{\gamma}, \quad (9)$$

where $\gamma > 0$ controls the sensitivity to task difficulty imbalance; higher values amplify gradient adjustments for harder tasks. Target gradient norms are:

$$\bar{G} = \frac{1}{2}(G_{\text{ctr}} + G_{\text{ord}}), \quad G_k^* = \bar{G} r_k(t). \quad (10)$$

The meta-objective is:

$$\mathcal{J}(\alpha | \theta) = |G_{\text{ctr}} - G_{\text{ctr}}^*| + |G_{\text{ord}} - G_{\text{ord}}^*| + \beta \mathcal{R}_{\text{ent}}(\alpha) \quad (11)$$

where $\beta \geq 0$ controls the strength of entropy regularization, encouraging balanced gating weights across samples. The entropy term is defined as:

$$\mathcal{R}_{\text{ent}}(\alpha) = -\frac{1}{B} \sum_{i=1}^B (w_{\text{ctr}}^{(i)} \log w_{\text{ctr}}^{(i)} + w_{\text{ord}}^{(i)} \log w_{\text{ord}}^{(i)}) \quad (12)$$

3.9 Optimization Procedure

Model parameters and meta-parameters are updated jointly as:

$$\theta \leftarrow \theta - \eta_{\theta} \nabla_{\theta} \mathcal{L}(\theta; \alpha), \quad \alpha \leftarrow \alpha - \eta_{\alpha} \nabla_{\alpha} \mathcal{J}(\alpha | \theta), \quad (13)$$

with positivity enforced via softplus reparameterization.

3.10 Training Procedure

Training is conducted in two stages using the same set of LoRA adapters. In the first stage, structured representation learning is performed by optimizing contrastive and ordinal objectives with gated

representations and MetaGradNorm-based loss balancing, shaping the latent space to reflect graded actionability. In the second stage, task-specific fine-tuning is applied to the same adapters without reinitialization, preserving the learned structure while adapting the model to downstream supervision.

4 Experiments

4.1 Experimental Setup

We conduct experiments on the A3CG dataset (Ong et al., 2025b), where each sample x_i is associated with a set of tuples:

$$\mathcal{L}_i \subseteq \mathcal{K} \times \mathcal{A}, \quad (14)$$

with \mathcal{K} denoting sustainability aspects or categories, and $\mathcal{A} = \{\text{indeterminate}, \text{planning}, \text{implemented}\}$ representing ordinal action levels. Evaluation follows a cross-category generalization protocol with disjoint training and test categories.

Contrastive Pair Construction. For each anchor i with labels \mathcal{L}_i , we define the intersection $I_{ij} = \mathcal{L}_i \cap \mathcal{L}_j$ with candidate j . Positive and negative sets are:

$$\begin{aligned} \mathcal{P}(i) &= \{ j \neq i \mid |I_{ij}| > 0 \}, \\ \mathcal{N}(i) &= \{ j \neq i \mid |I_{ij}| = 0 \}. \end{aligned} \quad (15)$$

Ordinal Pair Construction. Each \mathcal{L}_i is mapped to a dictionary $d_i : k \mapsto a$. For shared keys $\mathcal{K}_{ij} = \text{keys}(d_i) \cap \text{keys}(d_j)$, ordinal relationships are determined via a transition function:

$$\pi(a) = \begin{cases} \text{planning} & \text{if } a = \text{implemented}, \\ \text{implemented} & \text{if } a = \text{planning}, \\ \text{planning} & \text{if } a = \text{indeterminate}. \end{cases} \quad (16)$$

A candidate j is a positive ordinal sample if $\exists k \in \mathcal{K}_{ij}$ such that $d_j(k) = \pi(d_i(k))$; all others are negatives.

4.2 Models

We evaluate our approach on a diverse set of pre-trained open-source language models: T5 (Raffel et al., 2020), LLaMA-3-8B (Grattafiori et al., 2024), Mistral-7B (Jiang et al., 2023), Gemma-7B (Gemma Team et al., 2024), DeepSeek-7B (DeepSeek-AI et al., 2024b), and Qwen2.5-7B (Qwen et al., 2024). All models are used with frozen backbones and adapted exclusively via LoRA adapters following the same training protocol. Representations are extracted uniformly across

models, and the same adapters are optimized during both structured representation learning and subsequent task-specific fine-tuning.

4.3 Baselines and Ablation Study

We evaluate stability and cross-category generalization using a multi-fold protocol. First, we establish a control setting using standard balanced splits on the full dataset. For generalization, we adopt the A3CG three-fold protocol (Ong et al., 2025b), where specific aspect categories are withheld from training to form an unseen (US) test set, while disjoint samples from training categories form the seen (S) test set.

To isolate component contributions, we evaluate an increasingly expressive sequence of configurations. Starting from a LoRA-based PEFT baseline (Hu et al., 2022), we incrementally integrate contrastive learning (Khosla et al., 2020), ordinal supervision, gated feature modulation, and MetaGradNorm (Chen et al., 2018). All models are trained under identical conditions and evaluated at 4 and 6 epochs. This cross-fold strategy ensures a controlled analysis of robustness and performance gains across varying training regimes.

4.4 Evaluation Metrics

We use F1-score as the primary metric, focusing on AAA, and report results separately on seen (S) and unseen (US) test sets to evaluate generalization. To ensure stability, results are averaged across the three A3CG folds.

4.5 Implementation Details and Hyperparameter Tuning

We employ a staged tuning strategy on a fixed model and fold to ensure stability. We first calibrate the LoRA configuration and learning rate to establish a baseline (Schulman and Lab, 2025). We then independently tune the contrastive learning rate (Gao et al., 2021) and the ordinal margin m_0 (Liu et al., 2017) to balance structure and generalization. Subsequently, gating temperatures $T_{\text{ctr}}, T_{\text{ord}}$ and scaling parameters $\lambda_{\text{ctr}}, \lambda_{\text{ord}}$ are optimized to regulate relative loss influence. Finally, we tune MetaGradNorm parameters γ and β to stabilize multi-objective convergence (Chen et al., 2018). Final hyperparameters are fixed and applied consistently across all models and folds to ensure reproducibility and fair comparison.

5 Results and Discussion

We evaluate our framework on the AAA task, prioritizing robustness and cross-category generalization over in-distribution performance. Results are reported via F1-score on seen (S) and unseen (US) categories (Section 4).

5.1 Baseline vs Full Framework: Overall Robustness Trends

Table 1 demonstrates the effectiveness of COGLM, which integrates contrastive learning, ordinal loss, gating, scaling with lambdas and MetaGradNorm on the T5 architecture. COGLM consistently outperforms the standard T5 and previous A3CG baselines across all folds, achieving a peak overall AAA F1 score of 0.724 (Ong et al., 2025b). Notably, **the framework improves unseen category performance by 4 to 5 F1 points, confirming enhanced cross-category generalization**. These results indicate that jointly structuring representations and dynamically balancing objectives provides a superior inductive bias compared to isolated components, aligning with established research in structured representation learning (Kook et al., 2022; Wang et al., 2023).

Table 2 demonstrates that COGLM’s benefits extend to 7–8B decoder-only LLMs, consistently outperforming LoRA-only baselines. Notably, **COGLM-enhanced 7B models match or exceed the unseen-category performance of GPT-4o, Claude 3.5 Sonnet, and LLaMA-3-70B, despite having far fewer parameters**. While a gap between seen and unseen categories persists due to the complexity of ESG generalization, COGLM effectively improves performance on seen categories without any degradation in unseen results. These results confirm that structured, parameter-efficient adaptation provides a more effective inductive bias for transferable action-level representations than merely increasing model scale (Ong et al., 2025b; Wang et al., 2023).

These trends are further illustrated in Figure 1, which visualizes model trajectories in the joint space of seen performance, unseen performance, and $|\Delta|$ for Fold 1. As components are progressively added, models tend to move toward regions of higher unseen performance, but not always monotonically. **Robustness emerges gradually through representation structuring** rather than as a direct consequence of maximizing seen accuracy, and intermediate configurations often occupy

Table 1: T5 Results: Comparison between our method and A3CG baseline

Method	Full Dataset	Fold 1		Fold 2		Fold 3		S Avg	US Avg	Δ
		S	US	S	US	S	US			
T5	71.60	56.76	48.63	66.83	49.47	69.94	35.89	64.51	44.66	-19.85
T5 + COGLM	72.40	63.64	52.11	69.97	48.57	69.15	46.44	67.59	49.04	-18.55
T5 (A3CG)	70.48	57.85	43.03	68.90	45.74	67.94	34.59	64.90	41.12	-23.78
T5 + CL (A3CG)	71.12	62.96	46.97	69.76	46.67	67.99	38.33	66.90	43.99	-22.91

Table 2: LLM Results: Fine-tuned models (LoRA)

Method	Full Dataset	Fold 1		Fold 2		Fold 3		S Avg	US Avg	Δ
		S	US	S	US	S	US			
<i>Fine-tuned (LoRA)</i>										
LLaMA-3-8B	0.5668	0.5095	0.4626	0.6181	0.4422	0.5972	0.3481	0.5749	0.4176	-0.1573
LLaMA-3-8B + COGLM	0.6075	0.5678	0.4109	0.6346	0.4566	0.6669	0.3665	0.6231	0.4113	-0.2118
Mistral-7B	0.5963	0.6191	0.3880	0.6248	0.5000	0.6264	0.3977	0.6234	0.4286	-0.1948
Mistral-7B + COGLM	0.6206	0.5794	0.3786	0.6317	0.4361	0.6510	0.3864	0.6207	0.4004	-0.2203
Gemma-7B	0.5937	0.5747	0.4510	0.5737	0.3985	0.6043	0.3580	0.5842	0.4025	-0.1817
Gemma-7B + COGLM	0.6379	0.5626	0.3974	0.6363	0.4400	0.6170	0.3497	0.6053	0.3957	-0.2096
DeepSeek-7B	0.3690	0.3261	0.3082	0.4952	0.3417	0.3902	0.3065	0.4038	0.3188	-0.0850
DeepSeek-7B + COGLM	0.4405	0.4425	0.2953	0.5204	0.3869	0.4547	0.3053	0.4725	0.3292	-0.1433
Qwen2.5-7B	0.5906	0.5203	0.4079	0.6161	0.4636	0.6109	0.4022	0.5824	0.4246	-0.1578
Qwen2.5-7B + COGLM	0.6006	0.5465	0.3440	0.6185	0.4387	0.6173	0.3902	0.5941	0.3910	-0.2031

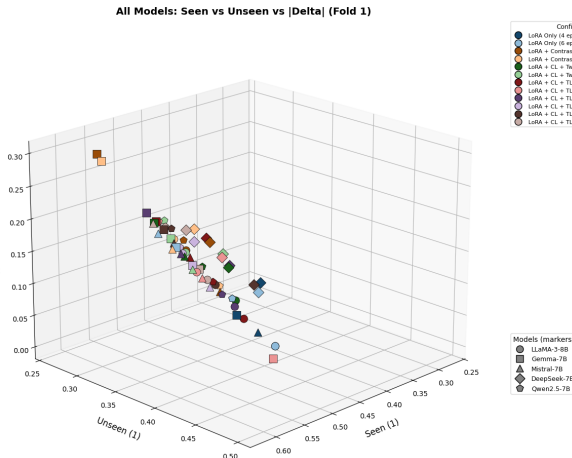


Figure 1: Seen vs Unseen vs $|\Delta|$ for Fold 1. Markers denote models; colors denote configurations.

favorable trade-off regions (Fu et al., 2022).

Distinct patterns emerge across model families: **encoder-decoder architectures, such as T5, tend to maintain a more stable balance between seen and unseen performance with smaller generalization gaps** dispersed trajectories, where gains in unseen performance can coincide with increased rigidity or higher variance. These findings reinforce the utility of analyzing robustness through the joint behavior of S, US, and Δ rather than relying on a single aggregate metric.

5.2 Progressive Component Contributions and Best Configurations

Figure 2 indicates that **the most effective configuration is not necessarily the most complex**. By reporting the configuration that maximizes a composite score $\text{Avg} - |\Delta|$, we observe that robustness appears to emerge from selective component composition rather than uniform application of all objectives (Zhou et al., 2024; Ploner and Akbik, 2024).

Trends vary significantly across folds: in Fold 1, models like Gemma-7B and Qwen2.5-7B reach their optimal trade-off using intermediate configurations (contrastive and ordinal supervision) without additional stabilization. In contrast, the full framework is more competitive in Fold 2 for several models. Fold 3 shows the highest variability, where some models benefit from minimal structure while others require stronger constraints to manage the generalization gap (Gorri et al., 2024; Yan et al., 2025). These results suggest that **the optimal structural balance is highly sensitive to the specific aspect categories encountered during training**.

Examination of component-level contributions clarifies these performance variations. While contrastive learning improves representation separation and unseen F1, it increases sensitivity to temperature and learning rates (Kim and Kim, 2025).

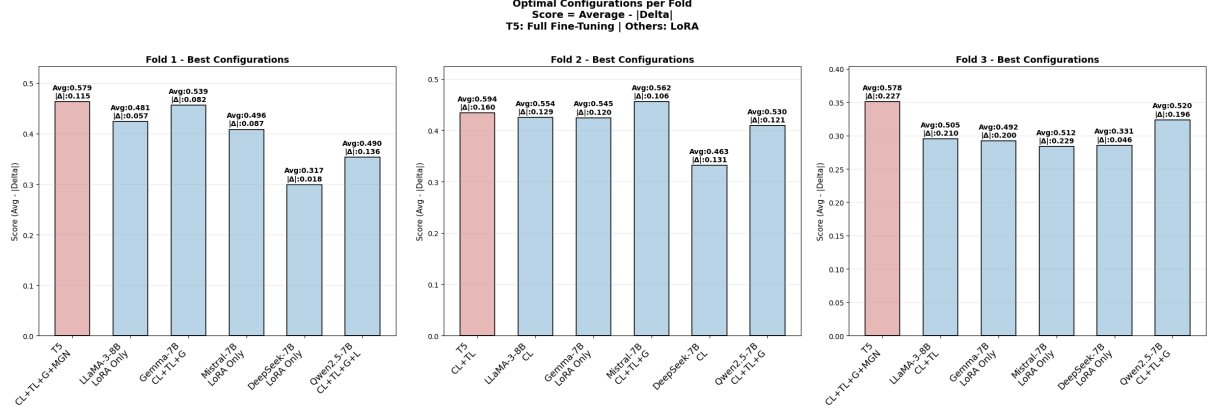


Figure 2: Best configurations comparison across folds for seen (solid) and unseen (hatched) categories. Each fold shows the F1 scores for the best-performing model on seen categories paired with its unseen performance, highlighting the generalization gap across different architectures.

Similarly, the ordinal loss provides task-aligned structure, but its effectiveness is highly sensitive to margin choice; excessive constraints can reduce model flexibility (Kim et al., 2024). Gated feature modulation improves stability by dynamically weighting dimensions, yet miscalibration of its scaling parameters can offset these gains (Qiu et al., 2025). Furthermore, MetaGradNorm balances competing gradients between contrastive and ordinal losses, though its impact varies across folds and can occasionally be less consistent than fixed-scaling mechanisms in lower-complexity settings (Chen et al., 2018).

Crucially, each component expands the hyperparameter surface. We observe that suboptimal tuning can cause simpler pipelines to outperform more complex configurations. These findings suggest that **robustness is not a direct function of methodological complexity but rather of the calibration between structured objectives and their hyperparameters**. Overall, effective generalization appears to arise from the balanced combination of components rather than maximal complexity alone.

5.3 Latent Space Structuring: Representation-Level Analysis

To complement our quantitative results, we examine how structured objectives influence latent space geometry. This analysis suggests that **gains in cross-category generalization are linked to shifts in embedding organization rather than optimization effects alone** (Ning and Rangaraju, 2025a). We focus on a representative case study from Fold 2 using the most stable model identified

in Section 5.2. This fold, which features diverse unseen categories, serves as an illustrative example of structured representation learning rather than a claim of uniform behavior across all settings.

Figure 3 compares PCA and UMAP projections of embeddings from the LoRA-only baseline and the optimal structured configuration (Kobak and Berens, 2023; Ning and Rangaraju, 2025b). **In the baseline, embeddings across different aspect categories are heavily intermixed.** Specifically, claims lacking explicit aspect annotations are scattered throughout the space, suggesting limited alignment between latent representations and the underlying action-level semantics.

In contrast, **the structured configuration exhibits a more organized geometry.** Operational categories, such as emissions control and waste management, form compact regions with clearer boundaries, while managerial aspects occupy more distinct areas (Islam and Fleischer, 2025). Claims without aspect labels concentrate into a localized region rather than diffusing across the space, suggesting improved separation between actionable and non-actionable content. These patterns are particularly coherent in the UMAP projection.

This visual reorganization is supported by clustering statistics: the structured configuration yields higher silhouette and Calinski–Harabasz scores, indicating tighter intra-cluster cohesion and improved inter-cluster separation (Calder and Lee, 2025; Grønbech et al., 2020). While these metrics are not directly optimized, their improvement aligns with the gains in unseen F1 on Fold 2. These findings suggest that **representation-level structuring may contribute to more transferable de-**

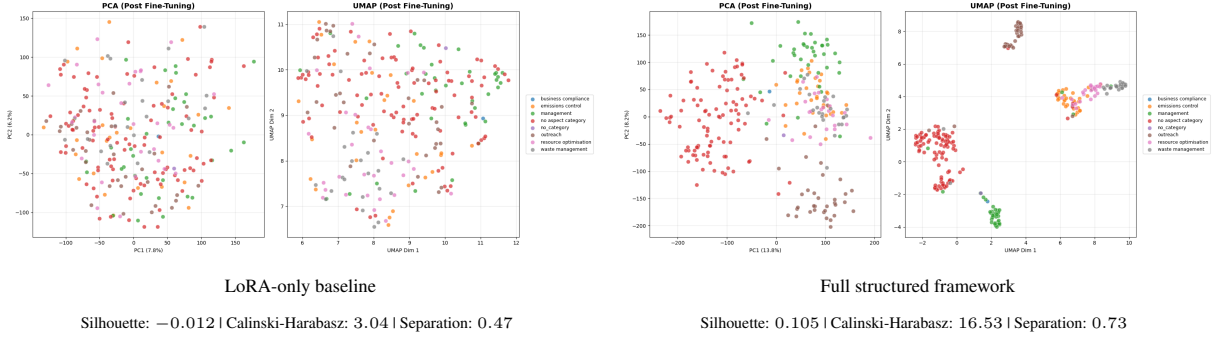


Figure 3: PCA and UMAP projections of latent representations for Mistral-7B on Fold 2. Left: Baseline shows diffuse clusters with low separation. Right: Full framework yields tighter, better-separated clusters by aspect category.

cision boundaries by reshaping the latent space in a manner consistent with action-level and category-level semantics.

5.4 Hyperparameter Sensitivity and Training Stability

The proposed framework introduces multiple interacting objectives and control mechanisms, making **performance highly sensitive to hyperparameter choices** (Tribes et al., 2023). To ensure that observed gains are not incidental, we conduct a staged hyperparameter analysis, illustrated through an extensive ablation study on LLaMA-3-8B, which we use as a representative case. This analysis highlights that **stable and robust performance emerges only when hyperparameters are tuned progressively**, following the order in which components are introduced (Wang et al., 2025).

At the base level, we observe substantial variability with respect to LoRA rank, scaling factor α , and fine-tuning learning rate. Even without additional objectives, inappropriate combinations can lead to unstable convergence or degraded unseen performance, indicating that **PEFT configuration alone already constrains the attainable robustness regime** (Zhang et al., 2025).

Introducing contrastive learning further increases sensitivity. **The contrastive learning rate plays a critical role:** overly large values can cause representation collapse, while overly small values limit separation benefits (Jeong et al., 2024). These effects are reflected in large fluctuations in unseen F1 across otherwise similar configurations. The addition of the ordinal objective introduces another critical parameter—the margin—which directly controls the rigidity of the induced ordering. **Margins that are too large enforce overly strict separation**, leading to reduced flexibility and a

systematic drop in unseen performance.

Gated feature modulation regulates latent dimension influence but introduces temperature and scaling parameters. If miscalibrated, gating may suppress useful gradients or amplify noise, potentially offsetting its intended stabilizing effect (Ou et al., 2025). At this stage, interactions between contrastive and ordinal objectives become fold-dependent, reflecting shifts in the semantic composition of unseen categories (Barker et al., 2025).

MetaGradNorm addresses these competing pressures at the optimization level by balancing conflicting gradients, thereby reducing inter-epoch instability and variance (Chen et al., 2018; Scetbon et al., 2025). However, our ablation results suggest that simpler stabilization mechanisms can yield more reliable performance if MetaGradNorm is poorly configured. These findings indicate that robust structured fine-tuning requires careful, staged hyperparameter control. Ultimately, **gains emerge not from methodological complexity alone, but from the precise joint calibration of structural objectives and their associated optimization landscapes**. Appendix D provides complete results.

6 Conclusion

We presented a structured, parameter-efficient framework for robust ESG claim analysis using action-level representations. On A3CG, combining contrastive and ordinal objectives with adaptive stabilization outperforms standard fine-tuning. Future work will address hyperparameter stability and transferability to reduce sensitivity across models and data splits.

Limitations

Our study is constrained by the A3CG benchmark, which is English-only and limited to a specific taxonomy of ESG aspects and three ordinal action levels. While our framework improves robustness, we observe that gains are not monotonic across folds and models: additional components increase the hyperparameter surface and can reduce generalization when miscalibrated. Moreover, our representation analysis relies on low-dimensional projections and clustering proxies that do not fully characterize decision boundary transfer. Finally, we focus on PEFT and a fixed training protocol; alternative objectives, sampling strategies, or data augmentation could change the observed trade-offs.

Ethical Considerations

We use publicly available corporate sustainability disclosures and follow the A3CG data governance and annotation guidelines. Although the texts may contain company or personal names, our analysis focuses on action-level content rather than individual profiling, and we avoid releasing any additional sensitive information beyond what is already public. All language models used in this study are open-source and openly accessible, selected to ensure transparency, reproducibility, and equitable access to research resources, and to avoid reliance on proprietary systems with opaque training data or constraints. We adhere to the licenses of all models, datasets, and software packages. Finally, as automated assessments of “actionability” may be misused as definitive credibility judgments, we position our framework as decision support and emphasize the need for human oversight and contextual interpretation.

References

Ramy Baly, Georgi Karadzhov, Abdelrhman Saleh, James Glass, and Preslav Nakov. 2019. Multi-task ordinal regression for jointly predicting the trustworthiness and the leading political ideology of news media. In *Proceedings of the 2019 Conference of the North American Chapter of the Association for Computational Linguistics: Human Language Technologies, Volume 1*, pages 2109–2116.

Matthew Barker, Andrew Bell, Evan Thomas, James Carr, Thomas Andrews, and Umang Bhatt. 2025. Faster, cheaper, better: Multi-objective hyperparameter optimization for llm and rag systems. *arXiv:2502.18635*.

Marco Bronzini, Carlo Nicolini, Bruno Lepri, Andrea Passerini, and Jacopo Staiano. 2024. Glitter or gold? deriving structured insights from sustainability reports via large language models. *EPJ Data Science*, 13(41).

Jeff Calder and Wonjun Lee. 2025. Understanding contrastive learning through variational analysis and neural network optimization perspectives. In *arXiv preprint arXiv:2503.10812*.

Zhao Chen, Vijay Badrinarayanan, Chen-Yu Lee, and Andrew Rabinovich. 2018. GradNorm: Gradient normalization for adaptive loss balancing in deep multitask networks. In *Proceedings of the 35th International Conference on Machine Learning (ICML)*, volume 80 of *PMLR*, pages 1200–1209.

DeepSeek-AI, Aixin Liu, Bei Feng, Bing Xue, Bingxuan Wang, Bochao Wu, Chengda Lu, Chenggang Zhao, Chengqi Deng, Chenyu Zhang, Chong Ruan, Damai Dai, Daya Guo, Dejian Yang, Deli Chen, Dongjie Ji, Erhang Li, Fangyun Lin, Fucong Dai, and 181 others. 2024a. Deepseek-v3 technical report. *arXiv preprint arXiv:2412.19437*.

DeepSeek-AI, Aixin Liu, Bei Feng, Bing Xue, Bingxuan Wang, Bochao Wu, Chengda Lu, Chenggang Zhao, Chengqi Deng, Chenyu Zhang, Chong Ruan, Damai Dai, Daya Guo, Dejian Yang, Deli Chen, Dongjie Ji, Erhang Li, Fangyun Lin, Fucong Dai, and 181 others. 2024b. Deepseek-v3 technical report. *arXiv preprint arXiv:2412.19437*.

Zihao Fu, Haoran Yang, Anthony Man-Cho So, Wai Lam, Lidong Bing, and Nigel Collier. 2022. On the effectiveness of parameter-efficient fine-tuning. *arXiv:2211.15583*.

Tianyu Gao, Xingcheng Yao, and Danqi Chen. 2021. SimCSE: Simple contrastive learning of sentence embeddings. In *Proceedings of the 2021 Conference on Empirical Methods in Natural Language Processing (EMNLP)*.

Gemma Team, Thomas Mesnard, Cassidy Hardin, Robert Dadashi, Surya Bhupatiraju, Shreya Pathak, Laurent Sifre, Morgane Rivière, Mihir Sanjay Kale, Juliette Love, Pouya Tafti, Léonard Huszenot, Pier Giuseppe Sessa, Aakanksha Chowdhery, Adam Roberts, Aditya Barua, Alex Botev, Alex Castro-Ros, Ambrose Slone, and 89 others. 2024. Gemma: Open models based on gemini research and technology. *arXiv preprint arXiv:2403.08295*.

Juan M Gorri, R. Martin Clemente, F Segovia, J Ramirez, A Ortiz, and J. Suckling. 2024. Is k-fold cross validation the best model selection method for machine learning ? *arXiv:2401.16407*.

Aaron Grattafiori, Abhimanyu Dubey, Abhinav Jauhri, Abhinav Pandey, Abhishek Kadian, Ahmad Al-Dahle, Aiesha Letman, Akhil Mathur, Alan Schelten, Alex Vaughan, Amy Yang, Angela Fan, Anirudh Goyal, Anthony Hartshorn, Aobo Yang, Archi Mitra, Archie Sravankumar, Artem Korenev, Arthur

Hinsvark, and 542 others. 2024. title=The Llama 3 Herd of Models,. *arXiv preprint arXiv:2407.21783*.

Christopher Heje Grønbech, Maximillian Fornitz Vording, Pascal N Timshel, Casper Kaae Sønderby, Tunc H Pers, and Ole Winther. 2020. scVAE: Variational auto-encoders for single-cell gene expression data. *Bioinformatics*, 36(16):4415–4422.

Zeyu Han, Chao Gao, Jinyang Liu, Jeff Zhang, and Sai Qian Zhang. 2024. Parameter-efficient fine-tuning for large models: A comprehensive survey. *Published in Transactions on Machine Learning Research*.

Yunchao He, Liang-Chih Yu, Chin-Sheng Yang, K. Robert Lai, and Weiyi Liu. 2016. YZU-NLP team at SemEval-2016 task 4: Ordinal sentiment classification using a recurrent convolutional network. In *Proceedings of the 10th International Workshop on Semantic Evaluation (SemEval-2016)*.

Edward J Hu, yelong shen, Phillip Wallis, Zeyuan Allen-Zhu, Yuanzhi Li, Shean Wang, Lu Wang, and Weizhu Chen. 2022. **LoRA: Low-rank adaptation of large language models**. In *International Conference on Learning Representations*.

Zizheng Huang, Haoxing Chen, Ziqi Wen, Chao Zhang, Huaxiong Li, Bo Wang, and Chunlin Chen. 2023. Model-aware contrastive learning: Towards escaping the dilemmas. In *Proceedings of the 40th International Conference on Machine Learning (ICML)*.

Mohammad Tariqul Islam and Jason W. Fleischer. 2025. The shape of attraction in umap: Exploring the embedding forces in dimensionality reduction. In *arXiv preprint arXiv:2503.09101*.

Yoo Hyun Jeong, Myeongsoo Han, and Dong-Kyu Chae. 2024. A simple angle-based approach for contrastive learning of unsupervised sentence representation. In *Findings of the Association for Computational Linguistics: EMNLP 2024*.

Albert Q. Jiang, Alexandre Sablayrolles, Arthur Mensch, Chris Bamford, Devendra Singh Chaplot, Diego de las Casas, Florian Bressand, Gianna Lengyel, Guillem Lample, Lucile Saulnier, Lélio Renard Lavaud, Marie-Anne Lachaux, Pierre Stock, Teven Le Scao, Thibaut Lavril, Thomas Wang, Timothée Lacroix, and William El Sayed. 2023. Mistral 7b. *arXiv preprint arXiv:2310.06825*.

Prannay Khosla, Piotr Teterwak, Chen Wang, Aaron Sarna, Yonglong Tian, Phillip Isola, Aaron Maschinot, Ce Liu, and Dilip Krishnan. 2020. Supervised contrastive learning. In *Advances in Neural Information Processing Systems (NeurIPS)*.

Bum Jun Kim and Sang Woo Kim. 2025. Temperature-free loss function for contrastive learning. In *arXiv:2501.17683*.

Daehwan Kim, Haejun Chung, and Ikbeom Jang. 2024. Calibration of ordinal regression networks. In *arXiv:2410.15658*.

Dmitry Kobak and Philipp Berens. 2023. The art of using t-SNE and UMAP for single-cell transcriptomics. *Nature Communications*, 10:5416.

Lucas Kook, Lisa Herzog, Torsten Hothorn, Oliver Dürr, and Beate Sick. 2022. Deep and interpretable regression models for ordinal outcomes. *Pattern Recognition*, 122:108263.

Vladislav Lialin, Vijeta Deshpande, Xiaowei Yao, and Anna Rumshisky. 2023. Scaling down to scale up: A guide to parameter-efficient fine-tuning. *arXiv preprint arXiv:2303.15647*.

Yanzhu Liu, Adams Wai Kin Kong, and Chi Keong Goh. 2017. Deep ordinal regression based on data relationship for small datasets. In *Proceedings of the 26th International Joint Conference on Artificial Intelligence (IJCAI)*.

Llama Team, AI @ Meta. 2024. The Llama 3 herd of models. *arXiv preprint arXiv:2407.21783*. Over 500 contributors.

Yuren Mao, Zekai Wang, Weiwei Liu, Xuemin Lin, and Pengtao Xie. 2022. MetaWeighting: Learning to weight tasks in multi-task learning. In *Findings of the Association for Computational Linguistics: ACL 2022*.

Alex Ning and Vainateya Rangaraju. 2025a. Visualizing ILM latent space geometry through dimensionality reduction. In *arXiv preprint arXiv:2511.21594*.

Alex Ning and Vainateya Rangaraju. 2025b. Visualizing ILM latent space geometry through dimensionality reduction. In *arXiv preprint arXiv:2511.21594*.

Keane Ong, Rui Mao, Ranjan Satapathy, Ricardo Shirota Filho, Erik Cambria, Johan Sulaeman, and Gianmarco Mengaldo. 2025a. Explainable natural language processing for corporate sustainability analysis. *Information Fusion*, page 102726.

Keane Ong, Rui Mao, Deeksha Varshney, Erik Cambria, and Gianmarco Mengaldo. 2025b. Towards robust ESG analysis against greenwashing risks: Aspect-action analysis with cross-category generalization. In *Proceedings of the 63rd Annual Meeting of the Association for Computational Linguistics (ACL)*.

Keane Ong, Rui Mao, Deeksha Varshney, Frank Xing, Ranjan Satapathy, Johan Sulaeman, Erik Cambria, and Gianmarco Mengaldo. 2025c. ESGSenticNet: A neurosymbolic knowledge base for corporate sustainability analysis. *arXiv preprint arXiv:2501.15720*.

Jie Ou, Shuaihong Jiang, Yingjun Du, and Cees G. M. Snoek. 2025. Gatera: Token-aware modulation for parameter-efficient fine-tuning. *arXiv:2511.17582*.

Tetyana Pimonenko, Yuriy Bilan, Jakub Horák, Liudmyla Starchenko, and Waldemar Gajda. 2020. Green brand of companies and greenwashing under sustainable development goals. *Sustainability*, 12(4):1679.

Max Ploner and Alan Akbik. 2024. Parameter-efficient fine-tuning: Is there an optimal subset of parameters to tune ? In *Findings of the Association for Computational Linguistics: EACL 2024*.

Zihan Qiu, Zekun Wang, Bo Zheng, Zeyu Huang, Kaiyue Wen, Songlin Yang, Rui Men, Le Yu, Fei Huang, Suozhi Huang, Dayiheng Liu, Jingren Zhou, and Junyang Lin. 2025. Gated attention for large language models: Non-linearity, sparsity, and stability. In *Advances in Neural Information Processing Systems (NeurIPS)*.

Weize Quan, Yunfei Feng, Ming Zhou, Yunzhen Zhao, Tong Wang, and Dong-Ming Yan. 2024. Tcan: Text-oriented cross attention network for multimodal sentiment analysis. In *arXiv:2404.04545*.

Qwen, :, An Yang, Baosong Yang, Beichen Zhang, Binyuan Hui, Bo Zheng, Bowen Yu, Chengyuan Li, Dayiheng Liu, Fei Huang, Haoran Wei, Huan Lin, Jian Yang, Jianhong Tu, Jianwei Zhang, Jianxin Yang, Jiaxi Yang, Jingren Zhou, and 25 others. 2024. Qwen2.5 technical report. *arXiv preprint arXiv:2412.15115*.

Colin Raffel, Noam Shazeer, Adam Roberts, Katherine Lee, Sharan Narang, Michael Matena, Yanqi Zhou, Wei Li, and Peter J. Liu. 2020. Exploring the limits of transfer learning with a unified text-to-text transformer. *Journal of Machine Learning Research*, 21(140):1–67.

Meyer Scetbon, Chao Ma, Wenbo Gong, and Edward Meeds. 2025. Gradient multi-normalization for stateless and scalable LLM training. In *Advances in Neural Information Processing Systems (NeurIPS)*.

John Schulman and Thinking Machines Lab. 2025. [Lora without regret](https://thinkingmachines.ai/blog/lora/). *Thinking Machines Lab: Connectionism*. [Https://thinkingmachines.ai/blog/lora/](https://thinkingmachines.ai/blog/lora/).

Yuan Song, Hongwei Wang, and Maoran Zhu. 2018. Sustainable strategy for corporate governance based on the sentiment analysis of financial reports with CSR. *Financial Innovation*, 4:1–14.

Dominik Stammbach, Nicolas Webersinke, Julia Anna Bingler, Mathias Kraus, and Markus Leippold. 2023. Environmental claim detection. In *Proceedings of the 61st Annual Meeting of the Association for Computational Linguistics (Volume 2: Short Papers)*.

Niklas Stoehr, Ryan Cotterell, and Aaron Schein. 2023. Sentiment as an ordinal latent variable. In *Proceedings of the 17th Conference of the European Chapter of the Association for Computational Linguistics (EACL)*.

Christophe Tribes, Sacha Benaroch-Lelong, Peng Lu, and Ivan Kobyzev. 2023. Hyperparameter optimization for large language model instruction-tuning. In *arXiv:2312.00949*.

Amir Pouran Ben Veyseh, Nasim Nour, Franck Dernoncourt, Quan Hung Tran, Dejing Dou, and Thien Huu Nguyen. 2020. Improving aspect-based sentiment analysis with gated graph convolutional networks and syntax-based regulation. In *Findings of the Association for Computational Linguistics: EMNLP 2020*.

Tongzhou Wang and Phillip Isola. 2020. Understanding contrastive representation learning through alignment and uniformity on the hypersphere. In *Proceedings of the 37th International Conference on Machine Learning (ICML)*.

Weiwei Wang, Wenyang Wei, Qingyuan Song, and Yansong Wang. 2023. Leveraging contrastive learning with bert for esg issue identification. In *Proceedings of the Fifth Workshop on Financial Technology and Natural Language Processing and the Second Multimodal AI For Financial Forecasting*.

Zhengbo Wang, Jian Liang, Ran He, Zilei Wang, and Tieniu Tan. 2025. LoRA-Pro: Are low-rank adapters properly optimized ? In *Proceedings of the 13th International Conference on Learning Representations (ICLR)*.

Wei Xue and Tao Li. 2018. Aspect based sentiment analysis with gated convolutional networks. In *Proceedings of the 56th Annual Meeting of the Association for Computational Linguistics (ACL)*.

Minghao Yan, Zhuang Wang, Zhen Jia, Shivaram Venkataraman, and Yida Wang. 2025. Plora: Efficient lora hyperparameter tuning for large models. *arXiv:2508.02932*.

Tianhe Yu, Saurabh Kumar, Abhishek Gupta, Sergey Levine, Karol Hausman, and Chelsea Finn. 2020. Gradient surgery for multi-task learning. In *Advances in Neural Information Processing Systems (NeurIPS)*.

Jun Zhang, Jue Wang, Huan Li, Lidan Shou, Ke Chen, Yang You, Guiming Xie, Xuejian Gong, and Kunlong Zhou. 2025. Train small, infer large: Memory-efficient lora training for large language models. In *arxiv:2502.13533*.

Han Zhou, Xingchen Wan, Ivan Vulić, and Anna Korhonen. 2024. AutoPEFT: Automatic configuration search for parameter-efficient fine-tuning. In *Transactions of the Association for Computational Linguistics, Volume 12*.

A A3CG Dataset Overview and Task Formulation

A.1 Dataset Structure

A3CG is a benchmark for aspect–action analysis of sustainability claims, where each claim may reference multiple ESG aspects and associated actions. Each claim is annotated with:

1. one or more *aspects*,
2. a higher-level *aspect category* grouping related aspects, and
3. an *action label* capturing the degree of concreteness and commitment expressed in the claim.

A.2 Ordinal Action Labels

Actions are organized along an ordinal scale reflecting increasing actionability and evidential grounding:

- **Indeterminate**: aspirational statements without concrete steps.
- **Planning**: future-oriented commitments or partial roadmaps.
- **Implemented**: actions described as carried out with verifiable details.

A.3 Cross-Category Generalization Setting

A3CG evaluates cross-category generalization by holding out a subset of aspect categories that are never observed during training or validation and are only evaluated at test time. Following prior work, we adopt a three-fold evaluation protocol, where each fold excludes a distinct set of aspect categories to form the unseen test split.

Since aspects from different categories frequently co-occur within the same claim, this setting differs from standard leave-one-domain-out evaluations. The protocol is therefore designed to minimize data leakage while preserving realistic statement composition, encouraging models to rely on transferable, action-centered representations rather than category-specific lexical cues.

A.4 Relevance to Structured Representation Learning

The ordinal structure of action labels and the cross-category evaluation protocol make A3CG well suited for studying structured representation learning. In this work, A3CG serves as a testbed for assessing whether contrastive and ordinal supervision can shape latent representations that generalize beyond seen sustainability categories. Table 3

provides representative examples illustrating the aspect–category–action annotation structure.

B Pair Construction Procedures

This appendix provides an algorithmic view of the pair construction procedures defined in Section 4 (Experimental Setup), translating Eqs. 15–16 into reproducible steps and clarifying implementation details.

B.1 Contrastive Pair Construction (Algorithmic Procedure)

Algorithm 1 implements the contrastive sampling rule in Eq. 15. For each anchor claim x_i , positives are all candidates whose label sets intersect with \mathcal{L}_i , and negatives are all remaining candidates. We exclude self-pairs ($j = i$) and construct multi-positive sets for the loss in Section 3.

Algorithm 1 Contrastive pair construction (multi-positive)

Require: Claims $\{x_i\}_{i=1}^N$ with label sets $\{\mathcal{L}_i\}$ (aspect- or category-level)

```
1: for  $i = 1$  to  $N$  do
2:    $\mathcal{P}(i) \leftarrow \emptyset$ ,  $\mathcal{N}(i) \leftarrow \emptyset$ 
3:   for  $j = 1$  to  $N$  do
4:     if  $j = i$  then
5:       continue
6:     end if
7:      $I_{ij} \leftarrow \mathcal{L}_i \cap \mathcal{L}_j$ 
8:     if  $|I_{ij}| > 0$  then
9:        $\mathcal{P}(i) \leftarrow \mathcal{P}(i) \cup \{x_j\}$ 
10:    else
11:       $\mathcal{N}(i) \leftarrow \mathcal{N}(i) \cup \{x_j\}$ 
12:    end if
13:   end for
14: end for
```

B.2 Ordinal Pair Construction (Algorithmic Procedure)

Algorithm 2 implements ordinal sampling using the transition function $\pi(\cdot)$ from Eq. 16. For each anchor x_i , we first map its label set \mathcal{L}_i into a dictionary $d_i : k \mapsto a$ (and similarly for x_j), where k denotes an aspect or category key. A candidate is an ordinal positive if it shares at least one key with the anchor and matches the expected transition for some shared key; otherwise it is assigned as a negative (including the case of no shared keys).

Algorithm 2 Ordinal pair construction (transition-based positives)

Require: Claims $\{x_i\}_{i=1}^N$ with label sets $\{\mathcal{L}_i\}$; transition $\pi(\cdot)$ (Eq. 16)

```

1: for  $i = 1$  to  $N$  do
2:    $d_i \leftarrow \text{DICT}(\mathcal{L}_i) \{k \mapsto a\}$ 
3:    $\mathcal{P}_{\text{ord}}(i) \leftarrow \emptyset$ ,  $\mathcal{N}_{\text{ord}}(i) \leftarrow \emptyset$ 
4:   for  $j = 1$  to  $N$  do
5:     if  $j = i$  then
6:       continue
7:     end if
8:      $d_j \leftarrow \text{DICT}(\mathcal{L}_j)$ 
9:      $\mathcal{K}_{ij} \leftarrow \text{keys}(d_i) \cap \text{keys}(d_j)$ 
10:    if  $\mathcal{K}_{ij} = \emptyset$  then
11:       $\mathcal{N}_{\text{ord}}(i) \leftarrow \mathcal{N}_{\text{ord}}(i) \cup \{x_j\}$ 
12:      continue
13:    end if
14:     $isPos \leftarrow \text{false}$ 
15:    for all  $k \in \mathcal{K}_{ij}$  do
16:      if  $d_j(k) = \pi(d_i(k))$  then
17:         $isPos \leftarrow \text{true}$ 
18:        break
19:      end if
20:    end for
21:    if  $isPos$  then
22:       $\mathcal{P}_{\text{ord}}(i) \leftarrow \mathcal{P}_{\text{ord}}(i) \cup \{x_j\}$ 
23:    else
24:       $\mathcal{N}_{\text{ord}}(i) \leftarrow \mathcal{N}_{\text{ord}}(i) \cup \{x_j\}$ 
25:    end if
26:  end for
27: end for

```

B.3 Aspect-Level vs. Category-Level Instantiation

The procedures above are identical for aspect-level and category-level construction; only the definition of the key space differs. In aspect-level mode, keys k correspond to fine-grained aspects. In category-level mode, aspects are first mapped to their parent categories, and keys correspond to categories. This mapping increases positive coverage (more shared keys per anchor) and encourages higher-level alignment across semantically related aspects, while preserving the same intersection and transition criteria.

B.4 Implementation Notes

Naïvely constructing pairs is $O(N^2)$ in the number of claims. In practice, we precompute dictionaries $\{d_i\}$ once, cache key sets $\text{keys}(d_i)$, and exclude self-pairs. All steps are deterministic given the dataset and the chosen granularity mode.

C Full Experimental Results

This appendix reports the complete set of experimental results for all evaluated models, folds, and training configurations. While the main paper focuses on representative trends and best-performing

configurations, the tables below provide exhaustive results to ensure full transparency and reproducibility.

C.1 Evaluation Protocol Recap

All results are reported in terms of F1 score for the Aspect–Action Analysis (AAA) task, evaluated separately on seen (S) and unseen (US) categories under the three-fold cross-category generalization protocol described in Section 4. For each configuration, we report results on all three folds as well as the full dataset, using the same format as Table 1 in the main paper.

C.2 T5 Configurations

For T5, we evaluate full fine-tuning as well as progressively structured configurations. The baseline fine-tuning setup uses a learning rate of 3×10^{-5} with a batch size of 8.

For contrastive learning, we perform a dedicated representation pre-training stage of up to 20 epochs with early stopping (patience = 3), using a learning rate of 1×10^{-4} , temperature $\tau = 0.07$, and a maximum of 2 positive and 2 negative samples per anchor with a batch size of 6.

Subsequent fine-tuning is conducted for 100 epochs, with the model checkpoint achieving the best validation performance selected for evaluation on the test set. For structured configurations beyond contrastive learning, we retain the same contrastive setup and incrementally introduce additional components. The ordinal loss is first added with a fixed margin of 0.05. For T5 specifically, gating and scaling are then applied simultaneously with $\lambda_c = 1.0$, $\lambda_o = 1.4$, $T_c = 5.8$, and $T_o = 1.0$. When MetaGradNorm is enabled, we use $\gamma = 0.5$, $\beta = 0.01$, and a meta-learning rate $\eta_{\text{meta}} = 0.001$ to adapt loss weights during training.

Table 10 reports full results for all T5 configurations across folds while Table 11 provides a direct comparison between the COGLM framework and previous methods utilized in A3CG.

C.3 Decoder-Only LLM Configurations

For decoder-only models (LLaMA-3-8B, Gemma-7B, Mistral-7B, DeepSeek-7B, and Qwen2.5-7B), we employ parameter-efficient fine-tuning with LoRA. Unless otherwise specified, all models use a LoRA rank of $r = 8$, scaling factor $\alpha = 16$, and LoRA dropout of 0.05.

Contrastive learning is performed with a batch size of 5, a maximum of 3 positive and 6 negative

samples per anchor, and 2 epochs of contrastive training. The contrastive learning rate is set to 1×10^{-4} .

Subsequent LoRA fine-tuning is carried out for a minimum of 4 and a maximum of 6 epochs, using a batch size of 3 and a learning rate of 3×10^{-5} . For progressively structured configurations, components are introduced in stages while keeping previously selected hyperparameters fixed. Gated feature modulation is first applied with temperatures $T_c = 13$ and $T_o = 1$, followed by loss scaling with $\lambda_c = 1$ and $\lambda_o = 2.5$. MetaGradNorm is then added with $\gamma = 0.5$, $\beta = 0.01$, and a meta-learning rate $\eta_{\text{meta}} = 0.001$. The temperature and scaling parameters are selected empirically based on the initial magnitude ratio between contrastive and ordinal losses, ensuring balanced gradient contributions during training.

Tables 4–8 provide exhaustive results for all decoder-only models across folds and configurations. Table 9 provides a direct comparison between the COGLM framework applied on LLMs and previous methods utilized with LLMs in A3CG.

C.4 Table Organization

Each table follows the same layout as Table 1 in the main paper, reporting: (i) the training configuration and (ii) fold-wise Seen and Unseen F1 scores. This organization enables direct comparison across models, folds, and methodological components, and allows the reader to trace performance variations back to specific architectural or optimization choices.

D Hyperparameter Study – LLaMA-3-8B

The staged exploration for LLaMA-3-8B is conducted according to the configurations detailed in Table 12. Initial LoRA baseline experiments vary rank and scaling pairs $(r, \alpha) \in \{(2, 4), (8, 16), (16, 32), (32, 64)\}$ with corresponding fine-tuning learning rates $\eta_{\text{FT}} \in \{6 \times 10^{-5}, 3 \times 10^{-5}, 2 \times 10^{-5}, 1.5 \times 10^{-5}\}$. Across all configurations, models undergo 2 epochs of contrastive pre-training followed by 4 epochs of supervised fine-tuning.

For the contrastive stage, the learning rate $\eta_{\text{contrastive}}$ is tested across $\{10^{-3}, 10^{-4}, 5 \times 10^{-5}\}$ while fixing $\eta_{\text{FT}} = 3 \times 10^{-5}$. Subsequent two-loss training introduces an ordinal margin $m_0 \in \{0.05, 0.10, 0.15\}$.

Gated configurations utilize temperature pairs $(T_c, T_o) \in \{(5, 4), (13, 1), (25, 0.5)\}$, followed by loss scaling coefficients $(\lambda_c, \lambda_o) \in \{(2, 1), (1, 2.5), (0.5, 5)\}$. Finally, MetaGradNorm stabilization is applied with parameters $\gamma \in \{0.2, 0.5, 1.0\}$, $\beta \in \{0.005, 0.01, 0.02\}$, and $\eta_{\text{meta}} \in \{3 \times 10^{-4}, 10^{-3}, 3 \times 10^{-3}\}$.

E Additional Visualizations

This appendix provides supplementary visualizations to extend the coverage of the analyses presented in Section 5. These figures are included for completeness and transparency, and do not introduce additional interpretations beyond those discussed in the main text.

E.1 Seen–Unseen Performance Trajectories Across All Folds

Figure 4 extends the three-dimensional visualization of seen performance, unseen performance, and $|\Delta|$ to all folds and model families. The figure reports trajectories for LoRA-based models and T5 full fine-tuning under identical plotting conventions, allowing inspection of fold-specific variability and configuration dispersion.

E.2 Additional PCA and UMAP Projections

Figure 5 presents PCA and UMAP projections of learned representations for Gemma-7B (Fold 1) and T5 (Fold 3). For Gemma-7B, we compare the LoRA-only baseline against LoRA + CL + TL + G, the second-best configuration on Fold 1, selected to illustrate embedding structure under a different model than T5. For T5, we compare the fine-tuning-only baseline against FT + CL + TL + G + L + MGN, the best-performing configuration on Fold 3.

F Implementation and Training Details

All experiments were conducted using publicly available frameworks, including PyTorch and the HuggingFace Transformers and PEFT libraries. Training was performed on NVIDIA A100 GPUs with 80,GB of memory, using mixed-precision (FP16) to reduce computational overhead. Optimization was carried out with AdamW, and reproducibility was ensured by fixing the random seed to 155 for Python, NumPy, and PyTorch. Training times were typically under one hour for T5 fine-tuning and approximately two hours for decoder-only LLM configurations, with early stopping applied during contrastive pre-training stages and

validation-based checkpoint selection used for final evaluation.

Claim (excerpt)	Aspect	Category	Action
“We aim to reduce our carbon footprint over the coming years.”	Emissions reduction	Environment	Indeterminate
“The company plans to invest in renewable energy infrastructure by 2026.”	Energy transition	Environment	Planning
“In 2023, we installed solar panels across all manufacturing sites.”	Renewable energy	Environment	Implemented

Table 3: Illustrative A3CG examples showing the aspect–category–action annotation structure.

Table 4: **LLaMA-3-8B — LoRA 8/16.** Abbreviations: CL=Contrastive, TL=Two Losses, G=Gating, L=Lambdas, MGN=MetaGradNorm.

Type	(Full)	Seen (1)	Unseen (1)	Seen (2)	Unseen (2)	Seen (3)	Unseen (3)
LoRA	0.5915	0.5095	0.4526	0.5908	0.4612	0.6373	0.3574
LoRA	0.5668	0.5095	0.4526	0.6181	0.4422	0.5972	0.3481
LoRA + CL	0.6195	0.5469	0.3700	0.6217	0.4450	0.6404	0.3529
LoRA + CL	0.6234	0.5588	0.3636	0.6186	0.4896	0.6965	0.3313
LoRA + CL + TL	0.6044	0.5078	0.4039	0.6000	0.3925	0.6202	0.3676
LoRA + CL + TL	0.6220	0.5594	0.3782	0.6191	0.4258	0.6096	0.4000
LoRA + CL + TL + G	0.6145	0.5530	0.4444	0.5798	0.4400	0.6272	0.3450
LoRA + CL + TL + G	0.6319	0.5884	0.4128	0.6290	0.4266	0.6411	0.3556
LoRA + CL + TL + G + L	0.6241	0.5469	0.4291	0.6048	0.4045	0.6102	0.3554
LoRA + CL + TL + G + L	0.6241	0.5803	0.3896	0.6309	0.4513	0.6564	0.3770
LoRA + CL + TL + G + L + MGN	0.6166	0.5459	0.4054	0.6364	0.4523	0.5971	0.3691
LoRA + CL + TL + G + L + MGN	0.6075	0.5678	0.4109	0.6346	0.4566	0.6669	0.3665

Table 5: **Gemma-7B — LoRA 8/16.** Abbreviations: CL=Contrastive, TL=Two Losses, G=Gating, L=Lambdas, MGN=MetaGradNorm.

Type	(Full)	Seen (1)	Unseen (1)	Seen (2)	Unseen (2)	Seen (3)	Unseen (3)
LoRA	0.5937	0.5747	0.4510	0.5737	0.3985	0.6043	0.3580
LoRA	0.5904	0.5885	0.3874	0.6048	0.4845	0.5921	0.3921
LoRA + CL	0.6192	0.5794	0.2825	0.5732	0.3888	0.5711	0.3531
LoRA + CL	0.6236	0.5887	0.2953	0.5909	0.4287	0.5979	0.3553
LoRA + CL + TL	0.5978	0.5912	0.3627	0.5485	0.4043	0.5934	0.3186
LoRA + CL + TL	0.6481	0.5741	0.3708	0.6382	0.4293	0.6070	0.3543
LoRA + CL + TL + G	0.6269	0.5728	0.3519	0.5466	0.4348	0.6068	0.3537
LoRA + CL + TL + G	0.6269	0.5798	0.4974	0.6226	0.4490	0.6403	0.3761
LoRA + CL + TL + G + L	0.6031	0.5842	0.3486	0.5166	0.3693	0.6073	0.3343
LoRA + CL + TL + G + L	0.6318	0.5795	0.4016	0.6137	0.4641	0.6159	0.3727
LoRA + CL + TL + G + L + MGN	0.6110	0.5714	0.3599	0.5714	0.4213	0.6135	0.3691
LoRA + CL + TL + G + L + MGN	0.6379	0.5626	0.3974	0.6363	0.4400	0.6170	0.3497

Table 6: **Mistral-7B — LoRA 8/16.** Abbreviations: CL=Contrastive, TL=Two Losses, G=Gating, L=Lambdas, MGN=MetaGradNorm.

Type	(Full)	Seen (1)	Unseen (1)	Seen (2)	Unseen (2)	Seen (3)	Unseen (3)
LoRA	0.5873	0.5394	0.4521	0.6248	0.5000	0.6264	0.3977
LoRA	0.5963	0.6191	0.3880	0.6248	0.5000	0.6264	0.3977
LoRA + CL	0.5587	0.5570	0.4184	0.6444	0.5000	0.6425	0.3955
LoRA + CL	0.6102	0.6136	0.4016	0.6380	0.4575	0.6517	0.3866
LoRA + CL + TL	0.6291	0.5828	0.3939	0.6306	0.4463	0.6173	0.3529
LoRA + CL + TL	0.6397	0.5998	0.4158	0.6247	0.4595	0.6486	0.3278
LoRA + CL + TL + G	0.6090	0.5583	0.3830	0.6145	0.5087	0.6667	0.3930
LoRA + CL + TL + G	0.6252	0.5877	0.4191	0.6263	0.4519	0.6572	0.3681
LoRA + CL + TL + G + L	0.6156	0.5912	0.3956	0.6137	0.4544	0.6145	0.3091
LoRA + CL + TL + G + L	0.6302	0.5915	0.4303	0.6299	0.4716	0.6590	0.3612
LoRA + CL + TL + G + L + MGN	0.6206	0.5794	0.3786	0.6317	0.4361	0.6510	0.3864
LoRA + CL + TL + G + L + MGN	0.6347	0.5990	0.3672	0.6130	0.4111	0.6431	0.3618

Table 7: **DeepSeek-7B — LoRA 8/16.** Abbreviations: CL=Contrastive, TL=Two Losses, G=Gating, L=Lambdas, MGN=MetaGradNorm.

Type	(Full)	Seen (1)	Unseen (1)	Seen (2)	Unseen (2)	Seen (3)	Unseen (3)
LoRA	0.3690	0.2727	0.2751	0.4190	0.2902	0.3540	0.3083
LoRA	0.3690	0.3261	0.3082	0.4952	0.3417	0.3902	0.3065
LoRA + CL	0.4434	0.3578	0.2663	0.4698	0.3045	0.4189	0.3219
LoRA + CL	0.4288	0.3862	0.2659	0.5284	0.3972	0.4501	0.3037
LoRA + CL + TL	0.4051	0.3788	0.3056	0.4474	0.3117	0.4525	0.3268
LoRA + CL + TL	0.4371	0.3414	0.2720	0.4802	0.3758	0.4800	0.3246
LoRA + CL + TL + G	0.4232	0.3572	0.2615	0.5170	0.3549	0.3921	0.3142
LoRA + CL + TL + G	0.4366	0.3666	0.2885	0.4825	0.3504	0.4652	0.3130
LoRA + CL + TL + G + L	0.4408	0.3604	0.2943	0.4747	0.3700	0.3361	0.2853
LoRA + CL + TL + G + L	0.4521	0.4543	0.3144	0.4890	0.3831	0.4475	0.2887
LoRA + CL + TL + G + L + MGN	0.4354	0.3127	0.2932	0.5021	0.3803	0.3721	0.2891
LoRA + CL + TL + G + L + MGN	0.4405	0.4425	0.2953	0.5204	0.3869	0.4547	0.3053

Table 8: **Qwen2.5-7B — LoRA 8/16.** Abbreviations: CL=Contrastive, TL=Two Losses, G=Gating, L=Lambdas, MGN=MetaGradNorm.

Type	(Full)	Seen	Unseen	Seen	Unseen	Seen	Unseen
		(1)	(1)	(2)	(2)	(3)	(3)
LoRA	0.5874	0.5203	0.4079	0.5931	0.4255	0.5405	0.3939
LoRA	0.5906	0.5203	0.4079	0.6161	0.4636	0.6109	0.4022
LoRA + CL	0.6262	0.5116	0.3413	0.5774	0.4417	0.5929	0.2963
LoRA + CL	0.6099	0.5309	0.3995	0.5788	0.3864	0.6170	0.3703
LoRA + CL + TL	0.6132	0.5330	0.3802	0.5954	0.4238	0.6254	0.3516
LoRA + CL + TL	0.6047	0.5227	0.3251	0.6301	0.4715	0.6471	0.3865
LoRA + CL + TL + G	0.5734	0.5483	0.4037	0.5910	0.4698	0.6121	0.3771
LoRA + CL + TL + G	0.6193	0.5593	0.3449	0.6144	0.4136	0.6182	0.4218
LoRA + CL + TL + G + L	0.6155	0.5580	0.4216	0.6340	0.4272	0.6117	0.3877
LoRA + CL + TL + G + L	0.5934	0.5669	0.3767	0.5990	0.4054	0.6371	0.3949
LoRA + CL + TL + G + L + MGN	0.6160	0.5236	0.3347	0.5980	0.4291	0.6198	0.3711
LoRA + CL + TL + G + L + MGN	0.6006	0.5465	0.3440	0.6185	0.4387	0.6173	0.3902

Table 9: LLM Results: Fine-tuned models (LoRA) and zero-shot/few-shot baselines

Method	Full Dataset	Fold 1		Fold 2		Fold 3		S Avg	US Avg	Δ
		S	US	S	US	S	US			
<i>Fine-tuned (LoRA)</i>										
LLaMA-3-8B	0.5668	0.5095	0.4626	0.6181	0.4422	0.5972	0.3481	0.5749	0.4176	-0.1573
LLaMA-3-8B + COGLM	0.6075	0.5678	0.4109	0.6346	0.4566	0.6669	0.3665	0.6231	0.4113	-0.2118
Mistral-7B	0.5963	0.6191	0.3880	0.6248	0.5000	0.6264	0.3977	0.6234	0.4286	-0.1948
Mistral-7B + COGLM	0.6206	0.5794	0.3786	0.6317	0.4361	0.6510	0.3864	0.6207	0.4004	-0.2203
Gemma-7B	0.5937	0.5747	0.4510	0.5737	0.3985	0.6043	0.3580	0.5842	0.4025	-0.1817
Gemma-7B + COGLM	0.6379	0.5626	0.3974	0.6363	0.4400	0.6170	0.3497	0.6053	0.3957	-0.2096
DeepSeek-7B	0.3690	0.3261	0.3082	0.4952	0.3417	0.3902	0.3065	0.4038	0.3188	-0.0850
DeepSeek-7B + COGLM	0.4405	0.4425	0.2953	0.5204	0.3869	0.4547	0.3053	0.4725	0.3292	-0.1433
Qwen2.5-7B	0.5906	0.5203	0.4079	0.6161	0.4636	0.6109	0.4022	0.5824	0.4246	-0.1578
Qwen2.5-7B + COGLM	0.6006	0.5465	0.3440	0.6185	0.4387	0.6173	0.3902	0.5941	0.3910	-0.2031
<i>Zero-shot / Few-shot</i>										
GPT-4o	0.2979	0.3161	0.4298	0.4000	0.3251	0.3558	0.3235	0.3573	0.3595	+0.0022
GPT-4o + FS*	0.3569	0.3908	0.4668	0.3912	0.4110	0.4005	0.3346	0.3942	0.4041	+0.0099
Claude 3.5 Sonnet	0.3770	0.3671	0.3944	0.4111	0.3688	0.4159	0.3822	0.3980	0.3818	-0.0162
Claude 3.5 Sonnet + FS*	0.4211	0.4062	0.4627	0.4318	0.4035	0.4504	0.3948	0.4295	0.4203	-0.0092
Llama 3 (70B)	0.2015	0.1797	0.2524	0.2366	0.1833	0.2231	0.1843	0.2131	0.2067	-0.0064
Llama 3 (70B) + FS*	0.2982	0.2503	0.3811	0.3349	0.3330	0.3315	0.2665	0.3056	0.3269	+0.0213
DeepSeek V3	0.4016	0.3806	0.4818	0.4527	0.4023	0.4246	0.3484	0.4196	0.4108	-0.0088
DeepSeek V3 + FS*	0.3563	0.3885	0.3016	0.4418	0.4451	0.4662	0.3443	0.4322	0.3637	-0.0685

Table 10: **T5.** Abbreviations: FT=Fine Tune, CL=Contrastive, TL=Two Losses, G=Gating, MGN=MetaGradNorm.

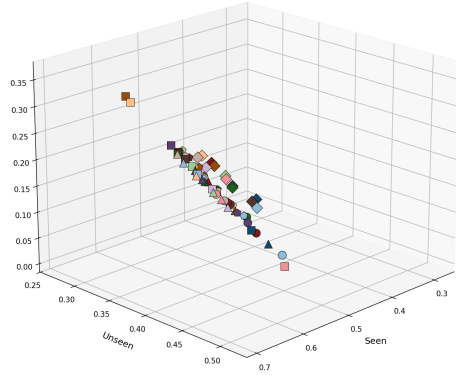
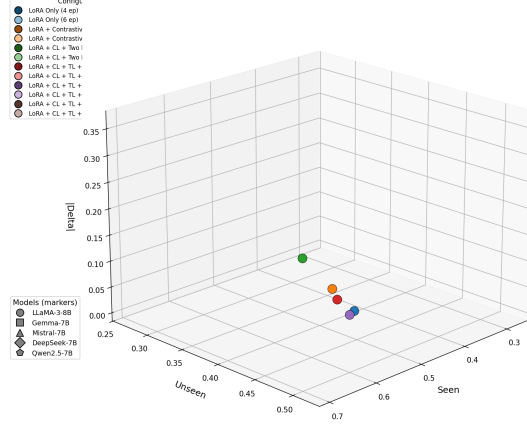
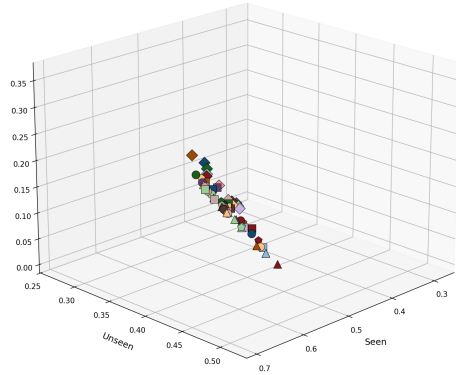
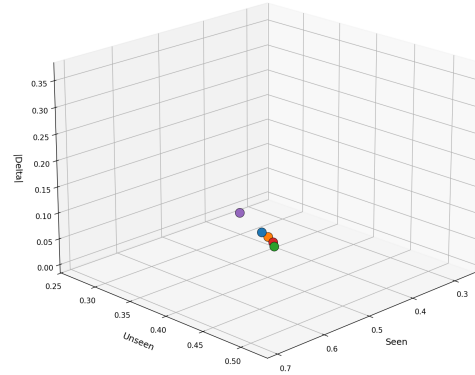
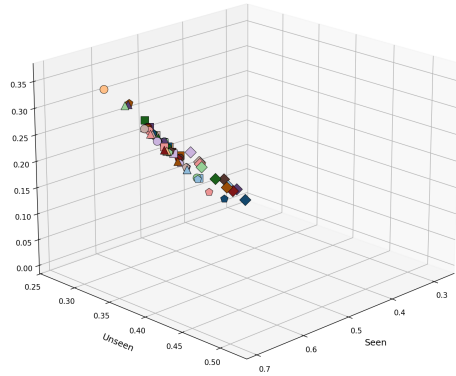
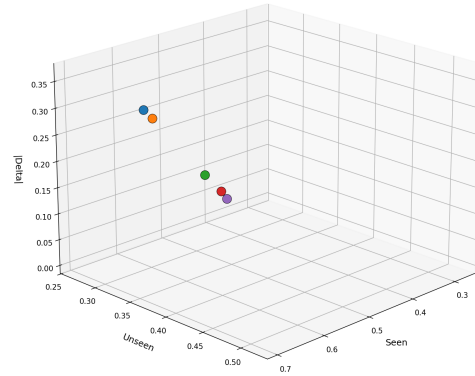
Type	(Full)	Seen	Unseen	Seen	Unseen	Seen	Unseen
		(1)	(1)	(2)	(2)	(3)	(3)
FT	0.7160	0.5676	0.4863	0.6683	0.4947	0.6994	0.3589
FT + CL	0.6955	0.5812	0.4657	0.6505	0.4921	0.6919	0.3660
FT + CL + TL	0.6943	0.5925	0.4332	0.6746	0.5141	0.6910	0.4353
FT + CL + TL + G + L	0.7172	0.6220	0.4967	0.6516	0.4988	0.6818	0.4508
FT + CL + TL + G + MGN	0.7240	0.6364	0.5211	0.6997	0.4857	0.6915	0.4644

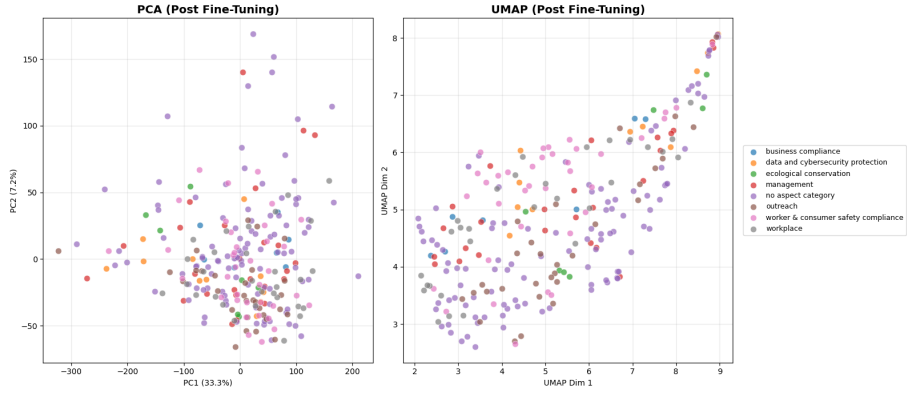
Table 11: T5 Results: Comparison between our method and A3CG baseline

Method	Full Dataset	Fold 1		Fold 2		Fold 3		S Avg	US Avg	Δ
		S	US	S	US	S	US			
<i>Ours</i>										
T5	71.60	56.76	48.63	66.83	49.47	69.94	35.89	64.51	44.66	-19.85
T5 + COGLM	72.40	63.64	52.11	69.97	48.57	69.15	46.44	67.59	49.04	-18.55
<i>A3CG Baselines</i>										
T5	70.48	57.85	43.03	68.90	45.74	67.94	34.59	64.90	41.12	-23.78
BERT-ST	43.19	39.56	25.25	39.00	22.92	43.97	30.01	40.84	26.06	-14.78
T5 + CL	<u>71.12</u>	<u>62.96</u>	<u>46.97</u>	<u>69.76</u>	46.67	<u>67.99</u>	38.33	<u>66.90</u>	<u>43.99</u>	-22.91
T5 + AL	69.27	61.24	39.62	66.91	<u>47.02</u>	65.17	<u>41.82</u>	64.44	42.82	-21.62
BERT-ST + CL	68.53	60.00	37.06	69.22	41.78	58.04	34.94	62.42	37.93	-24.49
BERT-ST + AL	24.30	37.75	27.05	27.13	25.57	34.70	26.11	33.19	26.24	-6.95
<i>Other ABSA Methods</i>										
InstructABSA	69.47	60.23	37.53	64.73	49.76	64.14	47.38	63.03	44.89	-18.14
IT-RER-ABSA	69.20	57.70	41.81	66.02	48.87	68.83	39.10	64.18	43.26	-20.96
GRACE	67.09	60.87	<u>50.08</u>	63.10	44.33	61.92	48.12	61.96	<u>47.51</u>	-14.45
CONTRASTE	71.33	<u>61.26</u>	48.14	69.81	50.30	71.34	40.58	<u>67.47</u>	46.34	-21.13

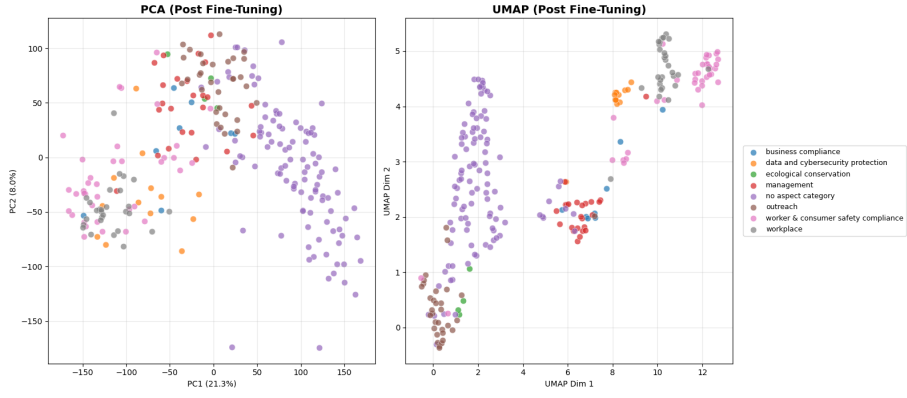
 Table 12: **LLaMA-3-8B (Hyperparameter tuning)**. Abbreviations: CL=Contrastive, TL=Two Losses, G=Gating, L=Lambdas, MGN=MetaGradNorm.

Type	Seen (1)	Unseen (1)
LoRA	0.5380	0.4439
LoRA	0.5095	0.4526
LoRA	0.5104	0.4830
LoRA	0.5193	0.4884
LoRA + CL	0.4513	0.3551
LoRA + CL	0.5469	0.3700
LoRA + CL	0.5365	0.3825
LoRA + CL + TL	0.5078	0.4039
LoRA + CL + TL	0.5362	0.3370
LoRA + CL + TL	0.5794	0.3812
LoRA + CL + TL + G	0.5489	0.4423
LoRA + CL + TL + G	0.5530	0.4444
LoRA + CL + TL + G	0.5188	0.4510
LoRA + CL + TL + G + L	0.5308	0.4525
LoRA + CL + TL + G + L	0.5469	0.4291
LoRA + CL + TL + G + L	0.5622	0.4239
LoRA + CL + TL + G + L + MGN	0.5459	0.4054
LoRA + CL + TL + G + L + MGN	0.5501	0.4190
LoRA + CL + TL + G + L + MGN	0.5223	0.4128

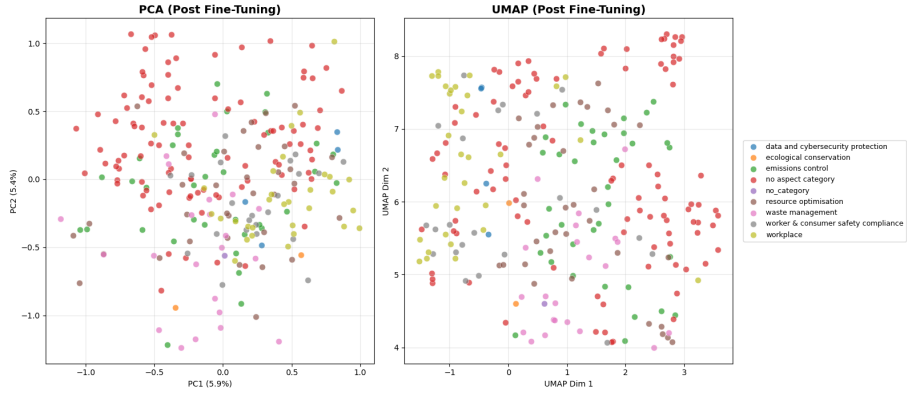
LoRA Models: Seen vs Unseen vs $|\Delta|$ (Fold 1)T5 (Full Fine-Tuning): Seen vs Unseen vs $|\Delta|$ (Fold 1)LoRA Models: Seen vs Unseen vs $|\Delta|$ (Fold 2)T5 (Full Fine-Tuning): Seen vs Unseen vs $|\Delta|$ (Fold 2)LoRA Models: Seen vs Unseen vs $|\Delta|$ (Fold 3)T5 (Full Fine-Tuning): Seen vs Unseen vs $|\Delta|$ (Fold 3)Figure 4: Seen vs. Unseen vs. $|\Delta|$ across all folds. Left: LoRA-based LLMs; Right: T5 full fine-tuning. Colors denote configurations; markers denote model backbones.



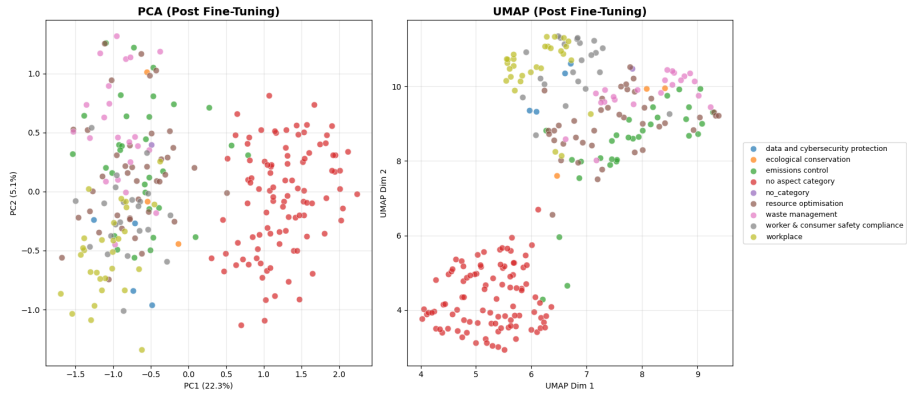
Gemma-7B: LoRA-only baseline | Sil.: -0.067 | CH: 2.47 | Sep.: 0.37



Gemma-7B: Full structured framework | Sil.: 0.082 | CH: 16.67 | Sep.: 0.79



T5: Fine-tuning-only baseline | Sil.: -0.030 | CH: 3.27 | Sep.: 0.52



T5: Full structured framework | Sil.: 0.047 | CH: 12.00 | Sep.: 0.62

Figure 5: PCA and UMAP visualizations for Gemma-7B (Fold 1, top) and T5 (Fold 3, bottom). Baselines show diffuse clusters; full frameworks yield tighter separation. Sil.=Silhouette, CH=Calinski-Harabasz, Sep.=Separation Ratio.